Geodesy and Geodynamics 11 (2020) 442–454

Contents lists available at ScienceDirect

Geodesy and Geodynamics

journal homepage: http://www.keaipublishing.com/geog

Atmosphere, ocean and lithosphere interaction as a possible drive of earthquake triggering

Victor Volkov [a], Jan Mrlina [b], Mstislav Dubrov [c, *], Vladimir Smirnov [c], Sergey Golovachev [c], Vaclav Polak [b]

[a] Schmidt Institute of Physics of the Earth of the Russian Academy of Sciences, Moscow, Russian Federation
[b] Institute of Geophysics of the Czech Academy of Sciences, Praha, Czech Republic
[c] Kotel'nikov Institute of Radioengineering and Electronics of the Russian Academy of Sciences, Fryazino, Russian Federation

ARTICLE INFO

Article history:
Received 6 October 2018
Accepted 26 July 2020
Available online 11 August 2020

Keywords:
Tilt and strain
Tropical cyclone
Earthquake
Hurricane

ABSTRACT

The comparison of tiltmeter and strainmeter data in the periods of the strongest earthquakes with tropical cyclone activities in the World Ocean during January–April 2014 is made. Main features of the observed co-seismic tilt and strain processes are consistent with the results obtained for the strongest events during 1997–2004. The time-frequency data analysis and the comparison of the analysis results with the anomalous geomagnetic and ionospheric activity come to an agreement with the observed phenomena. The obtained results have allowed the triggering mechanism of seismicity to be proposed. The process begins as spatial and temporal swings of the regions of tropical cyclone origins and the basins of their activity. The powerful cyclone development accompanies a wide range of earthquake precursory phenomena, including abnormal behavior of ultra-wideband (0.002 mHz–3 Hz) Earth's oscillations, which can be recorded at far distances up to 1000–10,000 km. The daily dissipation energy of the most powerful tropical cyclone (hurricane, typhoon) is estimated to have same order of magnitude as the energy released by an event of *M*w 7–9, as well, atmospheric depressions are big enough to trigger a forthcoming strong earthquake. The triggering mechanism could be caused by quasi-static and time-dependent surface loading that produces vertical tension and shear deformations. This loading affects the seafloor and coastline where they fall close to the adjacent tectonic plate boundaries.

1. Introduction

Pre-seismic and co-seismic abnormal occurrences recorded in upper lithosphere and hydrosphere layers as well as in atmosphere and ionosphere are the accompanying phenomena with all the strongest earthquakes and have ever been observed by geophysical instruments [1–3]. These appearances usually forerun or overlap the main shock in both preparatory and active phases of the earthquake cycle, therefore they are frequently defined as earthquake precursors [3,4].

The most common regularity of precursors are pre-seismic cave-shape variations of any observed geophysical parameters or a group of parameters, such as tilts and strains of earth surface, level of underground waters, atmosphere pressure and its composition, ionosphere electron concentration [5–8].

Another precursor can be the synchronization (correlation) of earth oscillations and background microseismicity. Such phenomenon, together with seismic quiescence prior to strong earthquakes, have been observed by numerous authors during past decades [3,6,9]. Analysis of tens of M_W7–8 events [9] has confirmed that close synchronization of spectral components of high frequency microseismicity (10–30 Hz) may precede strong earthquakes. The Earth's free oscillations (EFO) [10], especially their background noise (0.3–7.5 mHz) range, which are continuously

* Corresponding author.
E-mail address: mnd139@ire216.msk.su (M. Dubrov).
Peer review under responsibility of Institute of Seismology, China Earthquake Administration.

Production and Hosting by Elsevier on behalf of KeAi

https://doi.org/10.1016/j.geog.2020.07.001

excited even on seismically quiet days, are the research themes [11–14]. These oscillations were supposed to be forced by convective and turbulent atmospheric disturbances [15].

The increases of oscillation intensity at low and ultra-low frequency (ULF) band (0.05–0.5 mHz) have been found before a number of M_W7–8 earthquakes. ULF signals were registered on 18 April 1983 (Iran), 12 December 1992 (Indonesia), 11 May 1993 (Philippines), and 25 March 1998 (Balleni) by the spatially distributed seismo-gravimeters [12] and laser strainmeters [16].

All these processes were observed during the periods of low seismic activity, and the disturbances had been recorded before strong earthquakes [12,16]. Nevertheless, the nature of the all found phenomena was not enough understood until their interrelation with high powerful tropical cyclones (hurricanes, typhoons) in the World Ocean was assumed [17,18]. For example, the intensive strain-baric 0.05–0.07 mHz perturbations, being recorded 2 days before Balleny Islands M_W8.1 earthquake on 25 March 1998 [16], have been accounted for a row of severe tropical cyclones in South-Western (SW) region of Pacific and Indian Oceans [18,19]. The relationships between powerful typhoons in North-Western (NW) Pacific and the other two strong events of the Northern Hemisphere: Kronotskoe M_W7.8 on 5 December 1997 and Hokkaido M_W8.3 on 25 September 2003 earthquakes were analyzed [3,19]. Preliminary results of comparison of the tropical cyclone activity in Indian Ocean with catastrophic Sumatra M_W9.1, 26 December 2004 earthquake were reported [20].

In present paper, we offer the results of comparison of the data from geophysical instrument with tropical cyclones activities in the World Ocean, which occurred in the periods of the strongest earthquakes during 1997–2004. Time-frequency data analysis and its comparison with anomalous geomagnetic and ionospheric activities were carried out. The detail consideration of tiltmeter and strainmeter data together with tropical cyclones (typhoons) limited to the periods of the strongest earthquakes during January–April 2014 is presented. General characteristics of the observed co-seismic processes reiterate the conformity to the features obtained before a few M_W7–9 earthquakes.

2. Atmosphere-lithosphere interaction and ocean loading effects

Some geophysical processes involving earth surface deformations (e.g. tilts or strains) are always exposed to atmospheric changes. Tilt-baric and strain-baric coefficients, which characterize tilt-to-pressure (and strain-to-pressure) ratio, can decrease by about an order of magnitude when shallow measuring instruments were installed in underground galleries or tunnels [21]. Nevertheless, atmospheric pressure perturbations display their marked influence up to a depth of 1000 m [22,23]. In general, the atmospheric permanent circulation (convection, turbulence, vortices) induces observable tilt-baric and strain-baric disturbances of the Earth. Considering that oceans occupy more than 70% of the total globe surface, solar energy exchange processes above the World Ocean originally cause this circulation. The exchange processes form the distinguished part of atmosphere-ocean interactive energy, which is released in tropical cyclones activity. Therefore, the effects of this kind of ocean loading on the lithosphere as well as its coupling with geodynamic processes should be taken into consideration, which similarly accounts for the loading effects from the tides in oceans.

The direct solar irradiance at the top of the atmosphere is defined with the solar constant of 1.361 kW m^{-2} [24]. About a half of the solar energy actually reaches the Earth's surface. A certain part of this energy is absorbed by World Ocean and spent on heating and evaporation of ocean water, thus supporting the generation and development of a hurricane (typhoon). If an active zone of powerful tropical cyclone is assumed to be an order of $1.25 \cdot 10^{12}$ m^2 (active zone with a diameter about 1250 km corresponds to a powerful typhoon) and only 20% of the solar energy is transformed into a hurricane (typhoon) energy in the daytime, the power is about $1.7 \cdot 10^{14}$ W. The daily energy outcome of this rotating geophysical "engine" will be about $1.5 \cdot 10^{19}$ J, which is equivalent to the energy released by a strong earthquake of $M_W > 8.3$.

The most usual processes that continuously force the Earth's crust everywhere are microseisms. They occupy the wide frequency range from 10^{-2} Hz–10^2 Hz and have a natural origin as a rule. Such micro-seismic surface waves are generated by motion of the sea-floor associated with ocean waves. Microseisms with the periods of 1–5 s are excited by ocean surf and wind, while microseisms with the periods of more than 3–5 s are usually caused by large meteorological disturbances above oceans. Namely, the tropical cyclones were considered to be the sources of EFO (Earth's free oscillations) and ULF (Ultra-low frequency) oscillations even in a quiet period of seismicity [3,19].

As a rule, microseisms with frequencies higher than 1 Hz are excited by artificial sources and usually form the spatially distributed coherent seismic field. Abnormal evolutions of microseism spectrum and especially sharp synchronizations of microseism spectral components are frequently observed before strong earthquakes [9]. This phenomenon also should be accounted for by the interaction of atmosphere-ocean system with lithosphere due to tangible effects of this system loading on the lithosphere.

3. Instruments for tilt and strain measurements

Observation of ground tilts and strains enables one to estimate the spatial and temporal inhomogeneity of horizontal deformations of the Earth's crust. Note that the contribution of the Earth's elastic deformation to the direct tiltmeter signals reaches 30% for lunar and solar tides while this contribution to the gravimeter signals is several times smaller [20,25]. The ground based strainmeters, especially laser strainmeters, measure direct elastic deformations of the Earth's surface.

Powerful atmosphere-ocean processes and their interrelation with phases of the earthquake cycle can be revealed by direct observations of tilt and strain processes correlated with variating performances of adjacent liquid and fluid geospheres in the solid Earth. We have used the ground-based geophysical instruments combined with satellite radio techniques to observe these processes.

Two-component tiltmeter of NP–1M (Fig. 1) consists of sensor, control electronics, and recording equipment. Sensor, namely a vertical pendulum with a length of 100 mm, is mounted on the base with three adjustable screws. The main constituent elements are mounted in a case, which is protected by a sealed cap. The control unit can be connected to the sensor by signal cable with a length of 1 km. Tiltmeter measures the relative slopes of earth surface in two mutually perpendicular directions. Tiltmeter resolution is estimated as 1 milliarcsecond (mas) in tidal channel and 0.1 mas in seismic-accelerometer channel. Tiltmeter with horizontal pendulum installation has been also used in our observations [26]. The highest resolution of this instrument is estimated as 0.1 mas in tidal channel and 0.01 mas in seismic-accelerometer channel.

Selective results from tidal tilt observations in Pribram Observatory, which is situated in the Bohemian Massif, Czech Republic [27], are presented in Fig. 2.

Regular diurnal and semidiurnal tidal waves with peak-to-peak amplitude of about 20–30 mas are recorded during the quiet period of 7–10 September 2014 in Pribram (Fig. 2a). Linear trends of tilt signals vary between 3 and 8 mas per day and are shown as

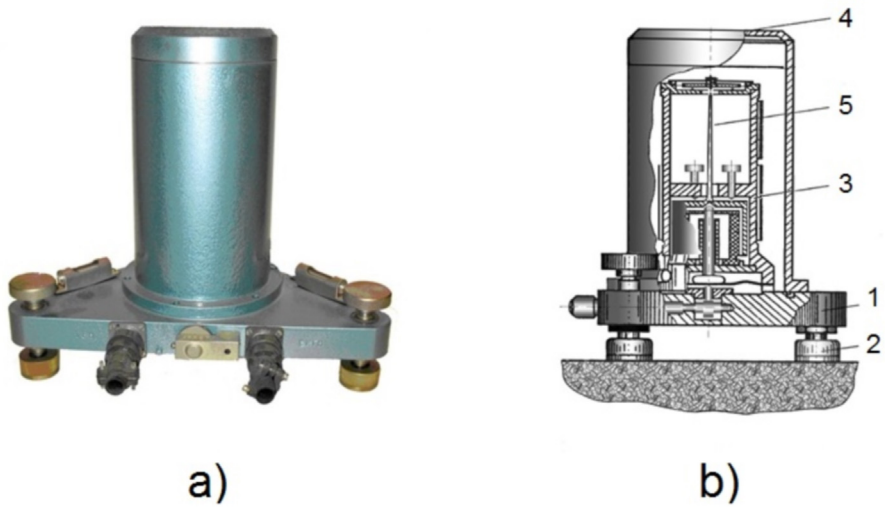

Fig. 1. General view (a) and instrumental design (b) of two-component NP–1M tiltmeter sensor: 1 – base, 2 – three adjustable feet, 3 – case with the main constituent elements, 4 – protective sealed cap, and 5–100 mm vertical pendulum.

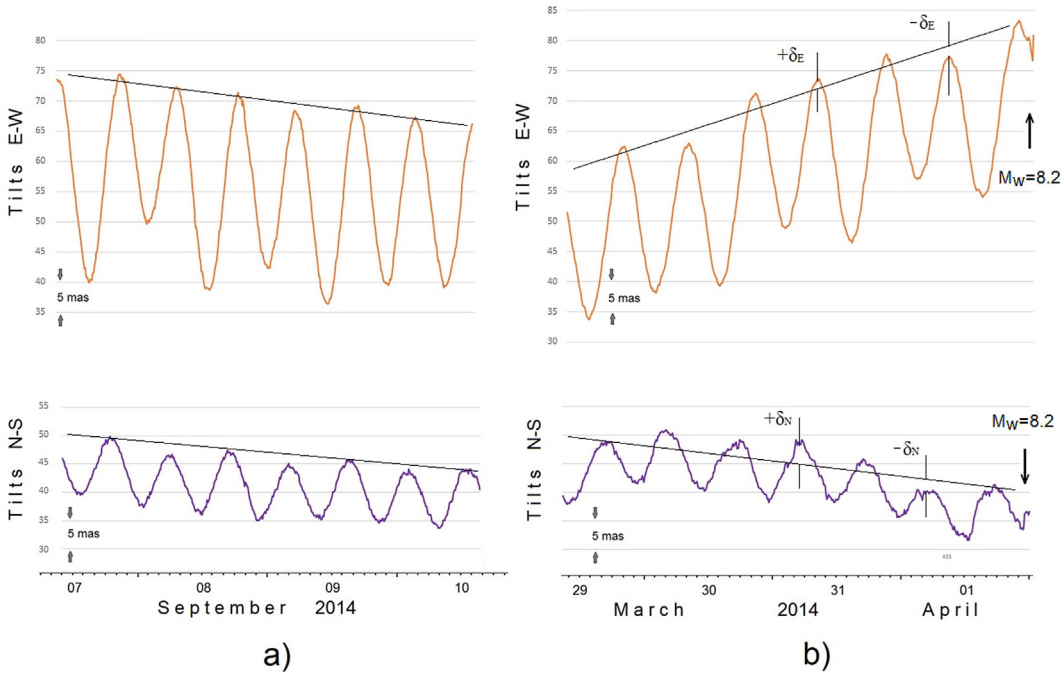

Fig. 2. E–W and N–S components of tidal tilts in Pribram Observatory at a depth of 90 m in old mine: a) records during the quiet period of 7–10 September 2014; b) pre-seismic E–W and N–S disturbances from 29 March to 01 April 2014. The E–W disturbance intensities are much smaller than the N–S ones.

straight lines in Fig. 2. Deviations of tilt signals from these linear trends are less than 1–2 mas in the quiet period (Fig. 2a). Pre-seismic ULF oscillations, mounting to 20–30% of amplitude of semidiurnal tides, are clearly seen in the disturbed period (Fig. 2b). The amplitudes of these non-tidal signals, which are denoted by $\pm\delta_E$ and $\pm\delta_N$ in Fig. 2b, are high enough to be measured without any filtering or other acquisition method.

Measurements of earth surface deformations were carried out by laser strainmeter installed at Fryazino testing site of Kotel'nikov Institute of Radioengineering and Electronics in Moscow region [21,23]. We used Michelson interferometer prototype with a 100 m-long arm enclosed in a 1.5–2 m underground steel pipe, which is filled with air and partially connected to the outer atmosphere. The instrument installation and equipment (Fig. 3) are similar to those of the 10 m airtight strainmeter, which was applied to investigate strain-baric processes [21]. An interferometer with an underground enclosure, being just partially air-tighten, gives an opportunity of observing dynamical interactions between earth surface and atmosphere [28].

The absolute resolution of strainmeter with precise recording system (Fig. 3b) was approved to be higher than 1 pm under 210 dB dynamic range in 0.8–1.2 Hz frequency band [29]. The highest relative strain resolution is $\Delta L/L = 10^{-11}$ –10^{-12} in the frequency range of 10^{-6}–10^{2} Hz. Typical value of thermal noise factor of about 10^{-8} K^{-1} is usually recorded for perfectly air-tighten interferometers. These instruments at the depths of 15–30 m in

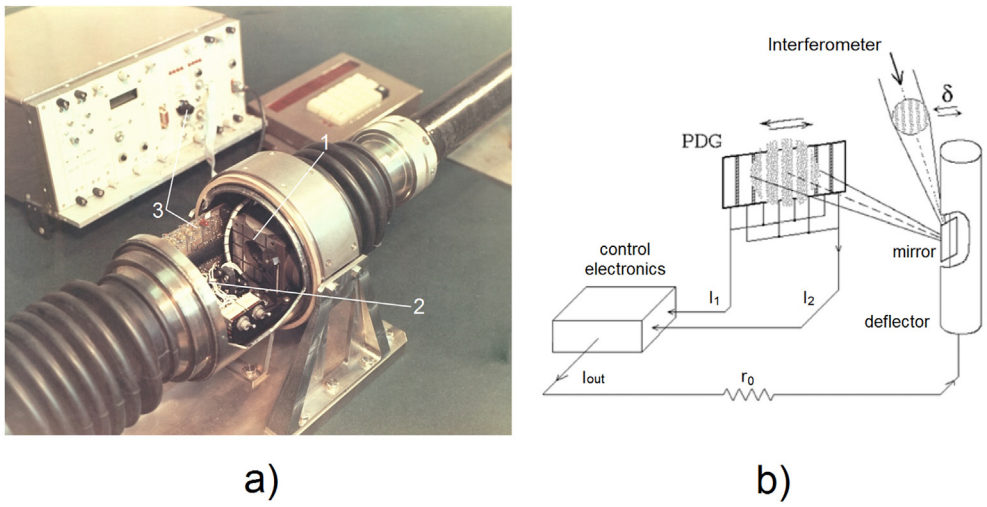

Fig. 3. General view (a) and block-diagram (b) of laser interferometer unit combined with precise recording system: 1 – interferometer, 2 – optical deflector, and 3 – control electronics, PDG – photodiode grating [29].

underground galleries [9,30] have characteristics which are comparable with the ones of uniquely evacuated terrestrial laser instruments [31–33] and those prototypes [34–37] installed 20 m–1 km below the ground surface.

Results from tiltmeter at Pribram observatory (Czech Republic) have been compared with strain-baric disturbances and seismic strain oscillations recorded by the interferometer at Fryazino site (Moscow region, Russia). In-phase and out-of-phase signal components are usually present by tilt α, strain L and atmospheric pressure P synchronously [21,28]. In Fig. 4a, strain-baric signal (Lp) is expressed as a linear function of L and P variations: $Lp = a \cdot dL + b \cdot dP$, therefore, Lp describes the combined instrument responses to earth strain and atmospheric pressure variations [28]. Seismic surface waves from China M_S7.1 (M_W6.9) earthquake, 12 February 2014 [38,39] are shown by the fragment of strain-baric signal (Lp) in Fig. 4a. Coherent synchronization of 1–3 Hz micro-seismic strains (dL) preceding the strong earthquake is shown in Fig. 4b. The evolution of micro-seismic strain coherency before the two strong Chile 2014 earthquakes is considered in Section 5.

4. Analysis of the earthquake-tropical cyclone coupling

Comparing the global tracks of powerful tropical cyclone (hurricane, typhoon) with the global distribution of earthquake epicenters, we can find a spatial correlation between earthquake and powerful cyclone occurrence in some particular regions of the World Ocean basins. A weak correlation in Northern Atlantics, a moderate correlation in South-Western (SW) Pacific or Indian Ocean and a high correlation in North-Western (NW) Pacific are observed. Hurricane tracks are frequently close to the plate boundaries in the Earth's crust. Due to the cold ocean flows in South-Eastern Pacific region, hurricanes are absent, so there is not

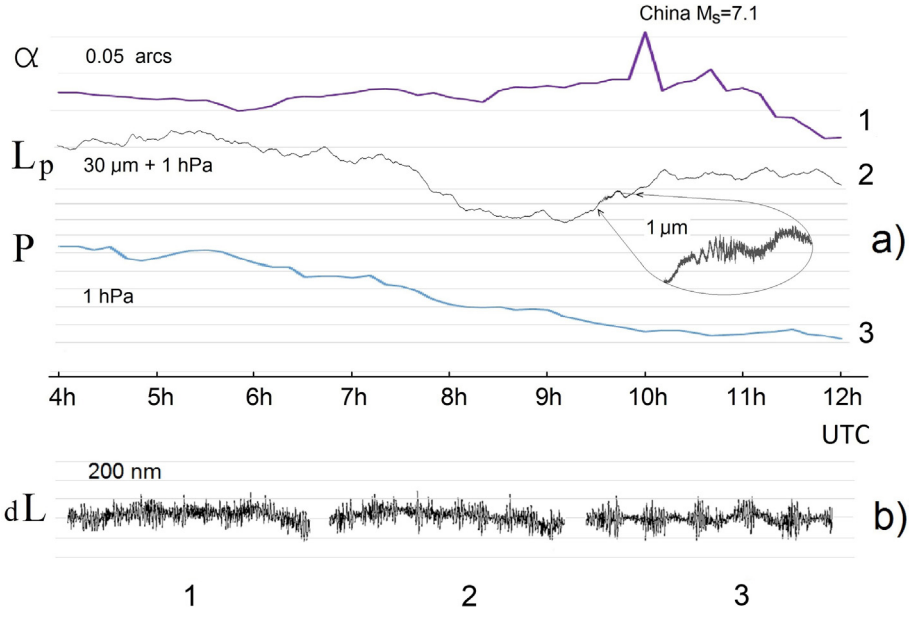

Fig. 4. Synchronous recordings of tilt (α), strain-baric (Lp, P) and seismic strain (dL) variations during 04:00–12:00 UTC on 12 February 2014. a) Tiltmeter (Pribram) installed in the observatory building at the ground surface level (1), laser strainmeter (Fryazino) with 100 m baseline (2), barometer in Pribram (3); b) coherency evolution of 1–3 Hz micro-seismic strains at Fryazino site, the recordings during ~1 min show no coherence (1), partial coherence (2) and high coherence (3).

any spatial correlation between earthquake and powerful cyclone occurrence in this basin.

The temporal correlation between tropical cyclones and earthquakes is more complicated and certain results were just a little discussed [19,40,41].

Below, we give the most prominent examples of the Category 1–5 (Saffir–Simpson hurricane wind scale) tropical cyclones [42,43], which were accompanied by those strongest earthquakes during 1997–2004. The considered cyclones and earthquakes are presented in Table 1 and Table 2 respectively.

4.1. Kronotskoe M_W7.8 earthquake (5 December 1997)

Kronotskoe M_W7.8 earthquake was the strongest earthquake in 1997. It occurred near East Coast of Kamchatka on December 5, 1997 [38]. The relationship between this interplate earthquake and super typhoon PAKA (Category 5 SSHWS, peak intensity 185 km/h, minimum pressure 920 mbar) [42,43] was considered [3]. The "bursts" of EFO oscillations were revealed 10–50 h before the earthquake according to the records from five broadband IRIS stations located 350–6800 km away from the epicenter.

However, there are two important notes here. (1) PAKA was strengthened little by little as tropical storm (63 km/h), remained until December 10, became a typhoon (wind speed > 118 km/h), and reached his peak (185 km/h, super typhoon) only near December 15 [43]. Therefore, this intensive atmosphere-ocean disturbance appeared after Kronotskoe earthquake. (2) On the other hand, more powerful super typhoons: KEITH (peak intensity 205 km/h, pressure 910 mbar), IVAN (peak intensity 195 km/h, pressure 905 mbar) and JOAN (peak intensity 195 km/h, pressure 905 mbar) were active in NW Pacific one and a half months ago. At the same time, a strong M_W7.5 intraplate earthquake occurred in Tibet on November 08, 1997 [39]. This event was accompanied with a rare cyclone transition from NW Pacific to North Indian Ocean basin. The typhoon LINDA (31 October – 9 November, Category 1) affected the southeastern tip of the Eurasian tectonic plate, hit the Malay Peninsula on November 3, then emerged into the Bay of Bengal, and was re-strengthened on November 4 [44].

Table 1
The most powerful tropical cyclones (typhoons, hurricanes) accompanied by the strongest earthquakes of 1997–2004, which are presented in Table 2 [42,43].

Name	Category	Duration	Basin
		1997	
JOAN	5	11–25 October	NW Pacific
IVAN	5	13–25 October	NW Pacific
KEITH	5	26 October–08 November	NW Pacific
LINDA	1	31 October–09 November	NW Pacific
PAKA	5	27 November–21 December	NW Pacific
		1998	
ANACELLE	4	05–14 February	Indian Ocean
VICTOR-CINDY	2	08–19 February	Indian Ocean
ELSIE	2	08–18 March	Indian Ocean
YALI	2	16–27 March	Southern Pacific
NATHAN	1	18–31 March	Australian region
ZUMAN	3	26 March–6 April	Southern Pacific
		2001	
ARB 01	3	21–28 May	Indian Ocean
ADOLPH	4	25 May–1 June	NE Pacific
CHEBI	3	19–23 June	NW Pacific
BARBARA	–	20–26 June	NE Pacific
		2003	
ETAU	3	02–09 August	NW Pacific
KROVANH	2	13–26 August	NW Pacific
DUJUAN	4	27 August–03 September	NW Pacific
MAEMI	5	05–13 September	NW Pacific
LINDA	1	13–17 September	NE Pacific
CHOI-WAN	3	16–23 September	NW Pacific
MARTY	2	18–24 September	NE Pacific
KOPPU	2	23–30 September	NW Pacific
NORA	2	01–09 October	NE Pacific
		2004	
AROLA	1	06–18 November	Indian Ocean
MUIFA	4	14–25 November	NW Pacific
BENTO	5	19 November–04 December	Indian Ocean
NANMADOL	4	29 November–04 December	NW Pacific
AGNI	1	27 November–04 December	Indian Ocean
TALAS	–	09–20 December	NW Pacific
NORU	–	16–22 December	NW Pacific
JUDY	1	21–27 December	Southern Pacific
SHAMBO	3	22 December–03 January	Indian Ocean
KERRY	3	05–14 January	Southern Pacific

4.2. Three strong earthquakes at the end of March 1998

The three strong earthquakes with different faulting mechanisms occurred in a 7-day interval at the end of March 1998. The epicenters of three earthquakes were located around Indo-Australian plate border (Fig. 5): Balleny Islands, M_W8.1, 25 March 1998; Tonga Islands, M_W7.2, 29 March 1998; and Southern Sumatra, M_W7.0, 1 April 1998 [38]. The M_W8.1 earthquake on 25 March was the strongest one near the Antarctic plate in 1998. The interaction of all these earthquakes with tropical cyclones in South Pacific and Indian Oceans has been explicitly analyzed [19].

It is necessary to pay attention to the important circumstance: one and a half months prior to the above-mentioned events, there was a Category 4 tropical cyclone ANACELLE (February 5–14) in SW Indian Ocean [43]. The cyclone's activity region is located at the conjunction of western edge of the Indo-Australian plate with Antarctic and African plates (see Fig. 5). This cyclone was the strongest one (peak intensity 205 km/h) during 1997–1998 South-West Indian Ocean cyclone season.

Another Category 2 tropical cyclone VICTOR-CINDY was formed in Australian region (Fig. 5) three days after ANACELLE starting. It moved westward, was intensified during 12–13 February, and then disappeared on February 19.

The next Category 2 storm – tropical cyclone ELSIE had been developed during 8–18 March 1998 in central region of SW Indian Ocean and reached its peak intensity with maximum wind velocities of 151–169 km/h. Further tropical activity has moved off to the SW Pacific region. Three tropical cyclones (YALI, 16–27 March 1998; NATHAN, 18–31 March 1998; and the most powerful ZUMAN, 26 March – 6 April 1998) had run in this basin. Note that the YALI's remnants moved towards the southern end of New Zealand and turned to the conjunction of Pacific, Indo-Australian and Antarctic plates, where Balleny M_W8.1 earthquake occurred.

The processes of interaction of tropical cyclones and earthquakes, which were shown here, happened in the following sequence. After dissipations of tropical cyclones in Indian Ocean, the origins of new storms were going on in SW Pacific basin (near the eastern edge of the Indo-Australian plate, see Fig. 5) and strong earthquakes accompanied this transition. Origin time and development of tropical cyclone YALI were synchronized with the beginning and intensifying of the strain-baric and gravity-baric activity in Moscow region respectively, which had been observed 2 days before M_W8.1 earthquake and recorded about 16,000 km away from the epicenters [16,19].

4.3. The strongest earthquake during 1999–2002 and the most powerful cyclones

The strongest earthquake during 1999–2002 occurred on June 23, 2001 (Peru, M_W8.4) [39]. Two powerful cyclones, namely severe cyclonic storm ARB 01 in Indian Ocean (Category 3, May 21–28)

Table 2
The major earthquakes (M_S, M_W = 7–9) in 1997–2004 according to CEME catalogs [38] and NEIC/USGS [39]; the yearly strongest earthquakes are distinguished in bold.

Date yy-mm-dd	Time (UTC) hh:mm:ss	Latitude	Longitude	Magnitude (CEME) (USGS) M_S	M_W	Region
1997-11-08	10:02:56	35.37° N	87.20° E	7.8	7.5	Tibet (Western Xizang)
1997-12-05	**11:26:54**	**54.86° N**	**162.0° E**	**7.9**	**7.8**	**Near East Coast of Kamchatka**
1998-03-25	**03:12:25**	**62.80° S**	**149.4° E**	**7.9**	**8.1**	**Balleny Islands Region**
1998-03-29	19:48:16	17.42° S	179.2° W	6.9	7.2	West of Tonga Islands
1998-04-01	17:56:22	0.50° S	99.30° E	7.0	7.0	Southern Sumatra
2001-06-23	**20:33:13**	**16.31° S**	**73.70° W**	**8.3**	**8.4**	**Near coast of southern Peru**
2003-09-25	**19:50:07**	**41.90° N**	**143,9° E**	**8.3**	**8.3**	**Hokkaido, Japan region**
2003-09-25	21:08:00	41.78° N	143.6° E	7.2	7.4	Hokkaido, Japan region
2003-09-27	11:33:26	50.03° N	87.78° E	7.3	7.3	Southwestern Siberia, Russia
2004-12-23	14:59:04	49.50° S	160.0° E	8.0	8,1	North of Macquarie Island
2004-12-26	**00:58:53**	**3.32° N**	**95.85° E**	**8.8**	**9.1**	**West coast of northern Sumatra**

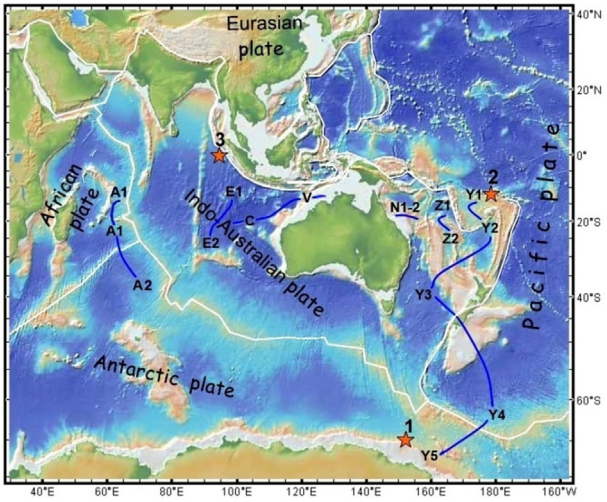

Fig. 5. The movements of tectonic plates were excited by tropical cyclones and the strongest earthquakes occurred during February–April 1998: A_{1-2} – ANACELLE, February 5–14; V–C – VICTOR-CINDY, February 8–19; E_{1-2} – ELSIE, March 8–18; Y_{1-5} – YALI, March 16–27; N_{1-2} – NATHAN, March 18–31; Z_{1-2} – ZUMAN, March 26 – April 6. Earthquakes: ★ Balleny Islands, M_W8.1, 25 March 1998; ★ Tonga Islands, M_W7.2, 29 March 1998; ★ Southern Sumatra, M_W7.0, 1 April 1998 (see Tables 1 and 2).

and hurricane ADOLPH in NE Pacific (Category 4, May 25 – June 1), opened the 2001 tropical cyclone season. The first cyclonic storm was the strongest one in the 2001 North Indian Ocean cyclone season. The consequent east-side and west-side excitations of Pacific plate were made by the tropical storm BARBARA (June 20–26) moving from Eastern to Central Pacific and typhoon CHEBI being active in Philippines – Taiwan region during June 19–23. BARBARA reached its peak (wind speed of 95 km/h) at noon on June 21, while CHEBI reached its peak (wind speed of 160 km/h) at 24:00 UTC on June 22 [44]. These processes appeared 2 days before the M_W8.4 interplate earthquake, which occurred near the coast of southern Peru at 20:33 UTC on June 23, 2001. The L1 and L2 (N–S and E–W components) photoelectrical tiltmeters, which operated at Lazec Observatory in South Bohemia, Czech Republic [27,45], recorded pre-seismic ULF oscillations of non-tidal signals with $\pm\delta_N$ and $\pm\delta_E$ amplitudes, amounting to 40–60% of semidiurnal tidal tilts during 18–22 June 2001 (Fig. 6).

4.4. Three strong earthquakes at the end of September 2003

The strongest interplate earthquake (M_W8.3, 19:50 UTC) and the second smaller shock (M_W7.4, 21:08 UTC) occurred in Hokkaido region on September 25, 2003; and the strongest of a series of intraplate earthquakes in Central Russia (Altai) was a M_W7.3 earthquake on September 27, 2003.

In August–September 2003, the regions of cyclone activities shifted alternately from eastern-northward to western-southward and vice versa in NW Pacific, exciting the boundary between Pacific and Eurasian tectonic plates. Typhoon ETAU (August 2–9, Category 3) hit the Japanese Islands and caused rainfall, triggering landslides, especially in Hokkaido [46]. The next three typhoons (KROVANH, DUJUAN and MAEMI) appeared. KROVANH (13–26 August, Category 2) went through Northern Philippines into the South China and Vietnam; DUJUAN (27 August–03 September, Category 4) passed near the southern tip of Taiwan and the east of Hong Kong; MAEMI (5–13 September, Category 5) ran northwestward from western Pacific into the East China Sea where it turned towards Japanese Islands. Near its peak intensity (195 km/h, 910 mbar), MAEMI traveled across Philippines-Eurasian plate boundary, passed through South Korea and emerged into the Sea of Japan.

Further weakening NW Pacific (NWP) typhoons (CHOI-WAN, Category 2 and KOPPU, Category 1) were followed by the corresponding North-Eastern Pacific (NEP) hurricanes: MAEMI (NWP) → LINDA (NEP, Category 1); CHOI-WAN (NWP) → MARTY (NEP, Category 2); and KOPPU (NWP) → NORA (NEP, Category 2) between the end of September and the beginning of October.

The cyclonic activity decreased during 25–27 September 2003, and gap in this activity was just filled by the strongest interplate (Hokkaido, M_W8.3) and intraplate (Altai, M_W7.3) earthquakes similar to the examples presented in Sections 4.1 and 4.2. A number of unusual geophysical processes – pre-seismic and co-seismic signals and anomalies were observed in adjacent geospheres. The abnormal behavior of seismic strain oscillations (earth deformations in seismic frequency range) in Moscow region (about 3000 km and 7000 km away from the epicenters) was limited to the period of 25–27 September [19]. Compared with its normal value a few days before and after the earthquakes, i.e. on September 22 and September 28, the ionospheric observations [28] from Tsukuba GPS station (Japan) showed a considerable increase (by 2–3 times) in the temporal variations of the total electron content (TEC) on September 24, 2003. At last, the intensive EFO (Earth's free oscillations) signals 9 days before Hokkaido M_W8.3 earthquake, recorded by IRIS net stations and mentioned by G.A. Sobolev [3], also indicate their probable relationship with abnormal phenomena.

KROVANH (Category 2) and DUJUAN (Category 4) typhoons mentioned above had excited the edges of the Eurasian tectonic plate in regions of Southern China and Vietnam. These excited disturbances are coupled with the intraplate Altai (27 September 2003) earthquakes and are very similar to the processes in the

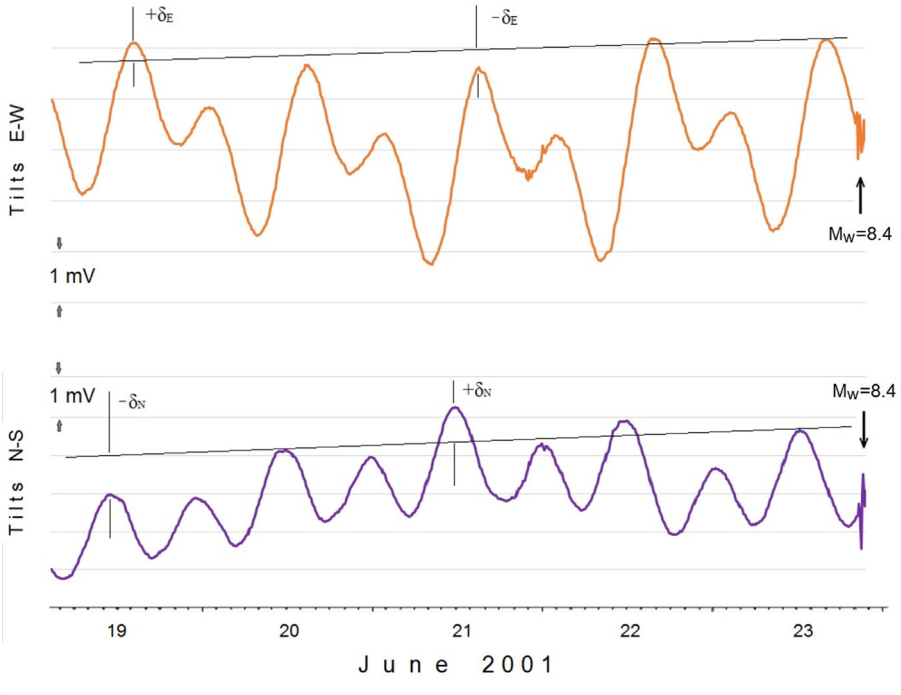

Fig. 6. The non-tidal pre-seismic ULF signals recorded by the L1 and L2 photoelectrical tiltmeters at Lazec Observatory in South Bohemia, Czech Republic during 18–22 June 2001.

beginning of November 1997, when typhoon LINDA affected the southeastern tip of the Eurasian tectonic plate before intraplate Tibet M_W7.5 earthquake (see Section 4.1).

4.5. Sumatra M_W9.1 and its predecessor – Macquarie M_W8.1 earthquake in 2004

Sumatra M_W9.1 on 26 December 2004 (00:58 UTC) earthquake and the preceding Macquarie M_W8.1 on 23 December 2004 (14:59 UTC) earthquake occurred in an interval of 3 days and attracted widespread attention [3,8,47]. Despite the quite different faulting mechanisms [48], two distinguished earthquakes occurred along the boundaries of the Indo-Australian plate.

Recordings from the tiltmeter at Jezeri Observatory, Czech Republic [27] in this period were used for analysis. Tiltmeter was installed in a gallery about 40 m underground. The observation site is located at a junction of Neogene clastic and fractured zone. Secular tilt trend is estimated to be about 2 arc-second/year in SW direction. Preliminary results of the Sumatra M_W9.1 and Macquarie M_W8.1 earthquakes were presented in our previous publication [20].

The tilt measurements from Jezeri Observatory in November–December 2004 were used for analysis and numerical processing. Peak-to-peak amplitudes of the semidiurnal tidal waves varied in the range of 0.2–0.4 mas and slightly irregular drifts of 0.1–0.2 mas per day were observed. The unfiltered tiltmeter data in December 2004 were linearized (Fig. 7a), and the linear tilt drift was removed from original records. Considerable intensive disturbances (80–120% of tidal amplitude) are distinctly visible at the regular background of diurnal and semidiurnal waves (Fig. 7a). Two months of data with a 10-min sampling rate were divided into fragments of 30-day duration. These fragments, each containing 4320 samples, were processed by computer program of time-frequency analysis with an analysis window 25% width.

The result of this analysis for data fragments on December 2004 is presented in Fig. 7b. The semidiurnal tides are distinguished on this diagram as the densely darkened spectral component at a frequency of near 0.022 mHz. The less intensive component at a frequency of near 0.012 mHz corresponds to the diurnal tides. Maximum tidal amplitudes vary between 0.02 and 0.04 units (see brightness column to the right of diagram) for diurnal and semidiurnal components. Especial disturbances with increasing frequencies from 0.002 mHz to 0.006 mHz are clearly seen during December 13–21, 2004 (inclined arrow in Fig. 7b). They mounted near tidal amplitude (up to 0.03 units) wherein the maximum of their amplitude appeared 5 days and 7 days before Macquarie M_W8.1 earthquake on 23 December 2004 and Sumatra M_W9.1 earthquake on 26 December 2004 (vertical arrows in Fig. 7a and b) respectively.

We carried out a comparison of these results with ionospheric monitoring data obtained by radio-translucence method using GPS–NAVSTAR navigation system in December 2004 [8]. Spatial and temporal distributions of ionospheric disturbances obtained from GPS observation in F2 layer were investigated in the areas close to Sumatra M_W9.1 earthquake epicenter (3.32° N, 95.85° E). The nearest ground-based station NTUS (Nanyang Technological University, Singapore) of the International GNSS Service network operated in 2004 was located about 1000 km away from the earthquake epicenter. Data from GPS receiver (AOA SNR-12 ACT, #225) were used. The satellite orbit altitude of ~20,000 km enables the trajectories of sub-ionospheric points on the terrain to be brought up to 180 km near the earthquake epicenter.

Spatial and temporal evolution of maximum values of electron concentration Ne_{max} obtained from GPS slant TEC by conjugate gradient method [49] in the F2 ionospheric layer is presented in Fig. 7c. Satellite radio-signals from GPS observation and procedure [49] were used to calculate the altitude profile of electron concentration, while the maximum values (Ne_{max}) of electron concentration are shown in Fig. 7c. One normalized unit NU corresponds to the conventional value of electron concentration: 1 NU $= 1 \cdot 10^6$ el/cm^3 in ionosphere. Data were derived from the daily observations of satellite #7 between 04:00 and 07:30 UTC during

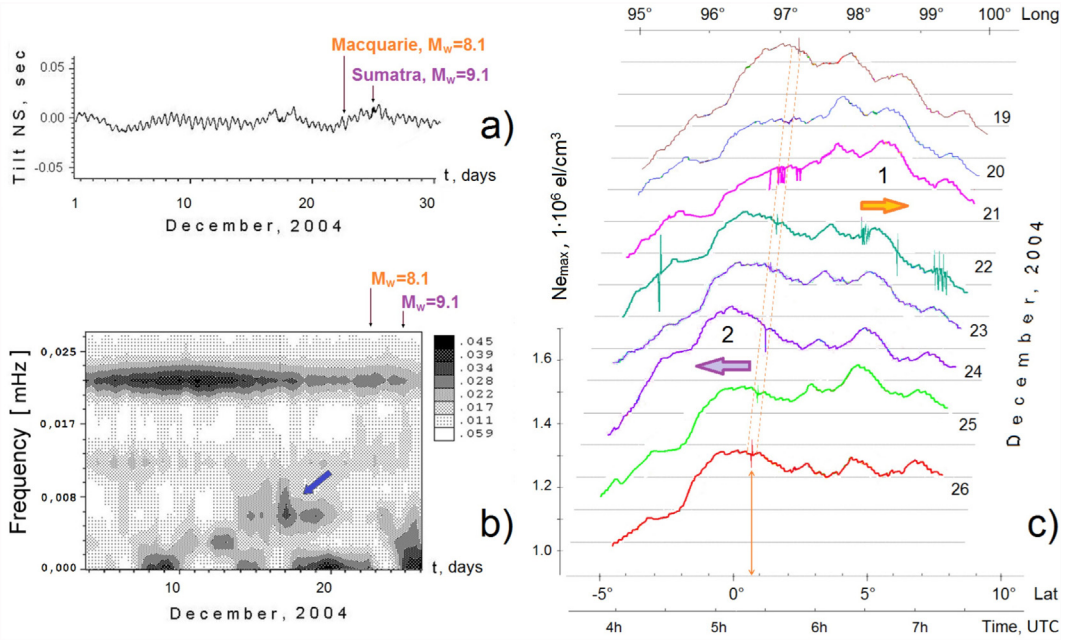

Fig. 7. Tiltmeter record at Jezeri Observatory during 1–30 December 2004 (a), time-frequency diagram during 4–26 December 2004 (b), and evolution of maximum values of electron concentration Ne_{max} obtained by gradient method [49] in the F2 ionospheric layer during 19–26 December 2004 wherein the horizontal arrows 1 and 2 indicate the distinguished modifications of Ne_{max} (c).

December 19–26, 2004. The results of Ne_{max} calculations are presented in Fig. 7c as a sequence of daily scans. The trajectories of sub-ionospheric points for satellite #7 lie in range of −5°~+8° latitude and 95°–100° longitude. The nearest point to the epicenter of Sumatra M_W9.1 earthquake has an approximate coordinates of [2.5° N, 97.5° E].

The obtained temporal-spatial distribution of electron concentration Ne_{max} has two particular spots during 06:00–07:00 UTC (98°–99° E) in December 21 and 04:00–05:00 UTC (~96° E) in December 24, which are shown by two horizontal arrows in Fig. 7c. The distinguished modifications of electron concentration by an order of 0.1–0.2 NU are observed at these spots. Note that the first spot (1) was observed 2 days before Macquarie M_W8.1 earthquake and the second spot (2) was observed 2 days before Sumatra M_W9.1 earthquake. We should also note the distortions of pulses shapes in Nemax results, showing a particular property of the temporal-spatial distribution of electron concentration in Fig. 7c. These distortions seem to be a source of obstacles in receiving radio-signals from satellite. The most intensive distortions in Ne_{max} results were observed on December 22, namely 1 day before Macquarie M_W8.1 earthquake and correspondingly 4 days before Sumatra M_W9.1 earthquake. Daily regular distortions of pulse shapes around 05:30 UTC and at ~1° N (denoted by dashed lines in Fig. 7c) can probably be explained by the trajectory of satellite sub-ionospheric points over subduction zone, which stretches about 150 km to the South of the Sumatra M_W9.1 earthquake epicenter.

Seven tropical cyclones (including two typhoons) and two tropical storms were active in Indian Ocean and Pacific basin during November–December 2004 (see Table 1) [42,43]. The most powerful cyclones in this period were BENTO (Category 5, SW Indian Ocean) and two typhoons (MUIFA, Category 4, NW Pacific and NANMADOL, Category 4, NW Pacific). Cyclone BENTO (19 November – 4 December 2004) was the strongest in 2004–2005 SW Indian Ocean cyclone season. BENTO ran to the West while MUIFA (November 14–25) and NANMADOL (28 November – 4 December) ran to the East of epicenter, and all of them were active about one month before Sumatra M_W9.1 earthquake. The spatial West – East and following East – West shifts of activity regions are inherent in all of the tropical cyclones, such as AGNI (Indian Ocean), TALAS and NORU (NW Pacific), SHAMBO (Indian Ocean), JUDY and KERRY (South Pacific).

It is noted that two interplate earthquakes (Macquarie M_W8.1 and Sumatra M_W9.1) occurred when NORU (exciting Pacific tectonic plate during 16–22 December) had dissipated and SHAMBO (being active above Indo-Australian plate during 23–28 December) had not yet reached its peak intensity. The similar performances were reproduced in previous four examples (Sections 4.1–4.4). The interesting is cyclone of the lowest intensity [50]. The cyclone JUDY (Category 1) during 21–27 December accompanied the Macquarie M_W8.1 earthquake alone, and the cyclone track as well as its development history seem to be sensitive to both the location and the time of the earthquake occurrence.

5. Physical and mathematical modeling interaction between tropical cyclone and earthquake

Previous analysis shows that the strongest earthquakes usually follow after the distinctly anomalous disturbances on earth surface as well as synchronous spatial and temporal perturbations in atmosphere and ionosphere. These perturbations have a spatial and temporal microstructure and are often accompanied by certain behaviors of tropical cyclones (hurricanes, typhoons). The abnormal lithosphere processes (to which the earthquake precursors are usually attributed) are overlapped with raising activities of atmosphere, hydrosphere (including underground water and World Ocean) and ionosphere. As a whole, it means there is a probabilistic relationship between development of tropical cyclones and seismogenic processes in the Earth's crust.

There is a certain temporal relation between earthquakes and tropical cyclones (hurricanes, typhoons), while their spatial correlation does not exist in all regions of the World Ocean. The epicenter of a strong accompanying earthquake can be far from active zone of cyclone. Tracks of tropical cyclones are sensitive to the fault distributions and subduction zones of the Earth's crust.

Track lines often indicate the way to the regions of future earthquakes. The resulting hurricane (typhoon) in stage of tropical disturbance sometimes leads to the spatial loops in hurricane track or abrupt displacements of hurricane center at the moment of earthquake occurrence [19]. This phase as a rule corresponds to the dissipation of the preceding cyclone in western (eastern) ocean basin and the origin of another cyclone in eastern (western) basin. Strong earthquake occurs in the gaps between western and eastern active regions of tropical cyclones. Similar processes may also develop when active regions of tropical cyclones are shifting in meridional direction from North to South or from South to North. With the advent of wideband microseisms, the "bursts" of EFO oscillations and ionospheric modifications happen. The fading amplitudes (or synchronization) of spectral components of seismic-acoustic precursors and ULF oscillations are observed by tiltmeter and strainmeter.

We preliminarily affirmed the interaction properties of atmosphere-ocean processes and strong earthquake. The detail comparison of the tiltmeter and strainmeter observation results with development of tropical cyclones in the World Ocean in the period of strongest earthquakes (January–April 2014) is presented below.

A few strong earthquakes (M_S, M_W > 7.0, Table 3) occurred in this period. Three of them (bold in Table 3) occurred at a time interval of 2.5 months (January 01 – February 29 and March 22 – April 04).

Two data sets for this period were analyzed and the results are shown in Figs. 8 and 9. The first series in January–February (Fig. 8a) was recorded by the tiltmeter, which is installed in surface building at Pribram Observatory. The second series in March–April (Fig. 9a) presents the data set from the deep tiltmeter in Pribram observational chamber, located in an old mine of 90 m underground and connected with the surface by inclined gallery [27].

Two-month (January–February) data set at a 10-min sampling interval was divided into two 30-day fragments and analyzed with the similar processing algorithm which was applied in Section 4.5. Each data fragment contains 4320 samples, therefore, each resulting time-frequency diagram consists of 3300 vertical line spectra if the analysis window size is 25% of the data fragment. This time interval corresponds to a 23-day duration. The accelerating drift of near 1.7 arc second/month and the wave of tilts with 1-week period of anthropogenic background signal were filtered and not taken into account in the analysis. The time-frequency analyses of these two fragments (04–26 January and 04–26 February) are presented in Fig. 8b. The analysis results were compared with anomalous geomagnetic perturbations in Moscow region [51] and tropical cyclone activity in Pacific and Indian Oceans [43,44], as shown in Fig. 8c.

Unstable tiltmeter operation and tidal tilt distortions can be seen at the beginning of the record in Fig. 8a. The unstable operation in form of short pulse obstacles on January 8–12 is correlated with the strengthening of the tropical cyclones in Southern Hemisphere: BEJISA (1), IAN (2) and COLIN (3) (see Fig. 8 and Table 4). They are organized as W–E sequence of cyclones 1–2 and E–W sequence of cyclones 2–3 (Fig. 8) and form the spatial swings of cyclone activity regions from Indian Ocean to Southern Pacific and from Southern Pacific to Indian Ocean. The tropical storms of unreached typhoon's intensity, namely LINGLING (NW Pacific) and JUNE (Southern Pacific), added SW–NE (3–4) and N–S components to the spatial swings respectively. Wideband disturbances of 0.07–0.13 mHz are clearly exhibited on the left time-frequency diagram during 7–16 January (Fig. 8b). The sharp overflow signal during 19–20 January correlates with LINGLING (4), DELIWE and JUNE storms, performing their synchronous dissipation in Indian and Pacific basins; the amplitude of ULF oscillations of 0.07–0.13 mHz band dropped down to its minimum level after these storms disappeared.

Calm weather has been going on for 9 days, and the following intensification of cyclonic activity (DYLAN, KAJIKI, FOBANE and other storms in Table 4 and Fig. 8) manifested as N–S (NW Pacific – Southern Pacific) and E–W (Southern Pacific – Indian Ocean) swings in the beginning of February. Finally, Category 1 tropical cyclone GUITO (6) occurred in the middle of this month. The evolution of tiltmeter ULF signals (see the right time-frequency diagram in Fig. 8b) is distinguished by the appearance of the densely darkened narrow-band spectral components in the middle of February, which indicate the synchronization of ULF oscillations in Pribram in this period. The intensive 0.08 mHz and 0.10 mHz oscillations began on February 10 and continued for a week. A series of geomagnetic storms (biggest storm, index K = 5) started on February 8 and continued until the end of February in Moscow Region [51]. The Xinjiang, China M_S7.1 (M_W = 6.9 according to NEIC/USGS web-catalog [39]) earthquake on 12 February 2014 was the strongest one in the preceding three months (November 2013–February 2014) (see Table 3 and Fig. 8).

Two precursors (tilt ULF oscillations and K = 5 geomagnetic storm) indicate the development of severe tropical storm FOBANE in Indian Ocean. The particular track of this cyclone goes just along the boundaries of African and Indo-Australian plates (Fig. 5), while Australian plate is contiguous to Southern Xinjiang, China (Table 3), where the M_S7.1 (M_W 6.9) intraplate earthquake occurred. Additionally, the spatial and temporal features of FOBANE's track seem to be sensitive to both the plate boundary direction and the occurrence time of the earthquake precursors [44].

In March–April 2014, considerable seismic activity ($M_W \geq 7$) shifted eastward: a series of strong earthquakes occurred in this period (Table 3). In total, eight interplate earthquakes occurred around Pacific plate: California, Chile (2 events), Solomon Islands (4 events), and Guerrero (Mexico). Northern Chile M_W8.2 earthquake

Table 3
M_S, $M_W \geq 7$ earthquakes in January–April 2014 according to CEME catalogs [38] and NEIC/USGS web-catalog [39].

Date	Time [UTC] hh:mm:ss	Latitude	Longitude	Magnitude [CEME] [USGS] M_S	M_W	Region
12 February	**09:19:47**	**36.00° N**	**82.61° E**	**7.1**	**6.9**	**Southern Xinjiang, China**
10 March	05:18:12	40.79° N	124.95° W	6.9	6.8	Near coast of Northern California
1 April	**23:46:44**	**19.45° S**	**70.75° W**	**7.9**	**8.2**	**Near coast of Northern Chile**
3 April	**02:43:10**	**20.63° S**	**70.90° W**	**7.6**	**7.7**	**Near coast of Northern Chile**
11 April	07:07:20	6.47° S	154.96° E	6.7	7.1	Solomon Islands
12 April	20:14:38	11.22° S	162.09° E	7.7	7.6	Solomon Islands
13 April	12:36:18	11.35° S	161.85° E	7.4	7.4	Solomon Islands
18 April	14:27:24	17.44° N	100.94° W	7.2	7.2	Guerrero, Mexico
19 April	13:27:58	6.72° S	154.94° E	7.4	7.5	Solomon Islands

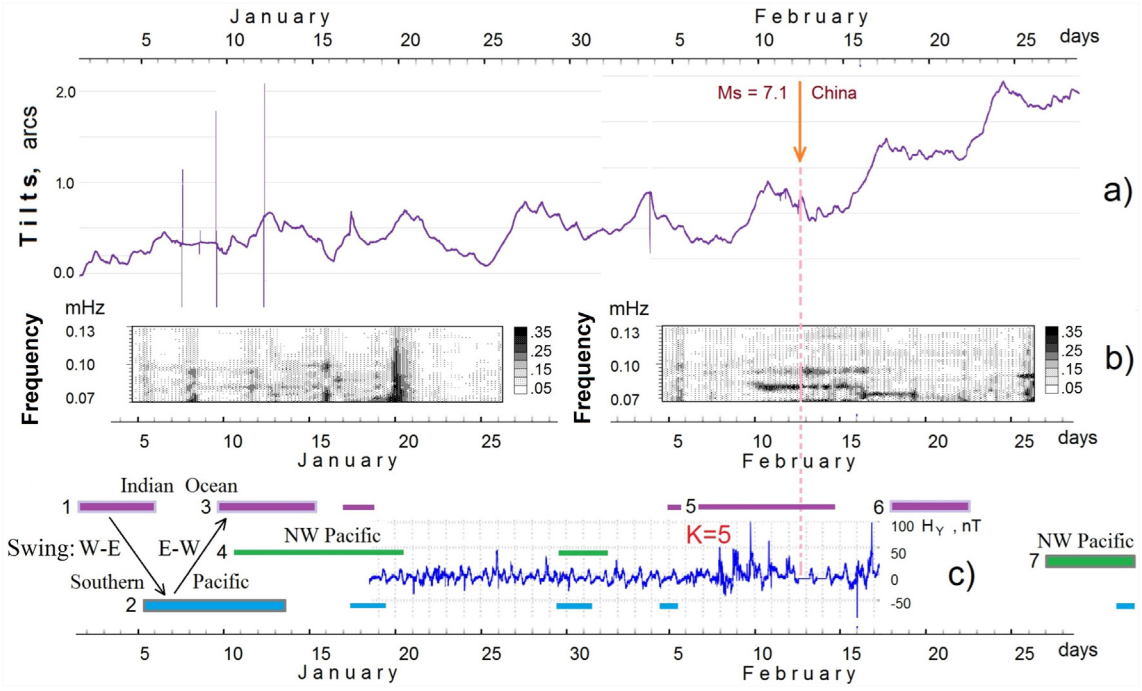

Fig. 8. Unfiltered tilt records from surface tiltmeter in Pribram (a) and their time-frequency diagrams (b); the pre-seismic $K = 5$ geomagnetic storms in Moscow Region (c). Tropical cyclone activities in Pacific and Indian Oceans in January–February 2014, intensive tropical cyclones: BEJISA - 1, IAN - 2, and COLIN - 3, storms: LINGLING - 4 and FOBANE - 5, cyclone GUITO - 6, and typhoon FAXAI - 7 (see Table 4).

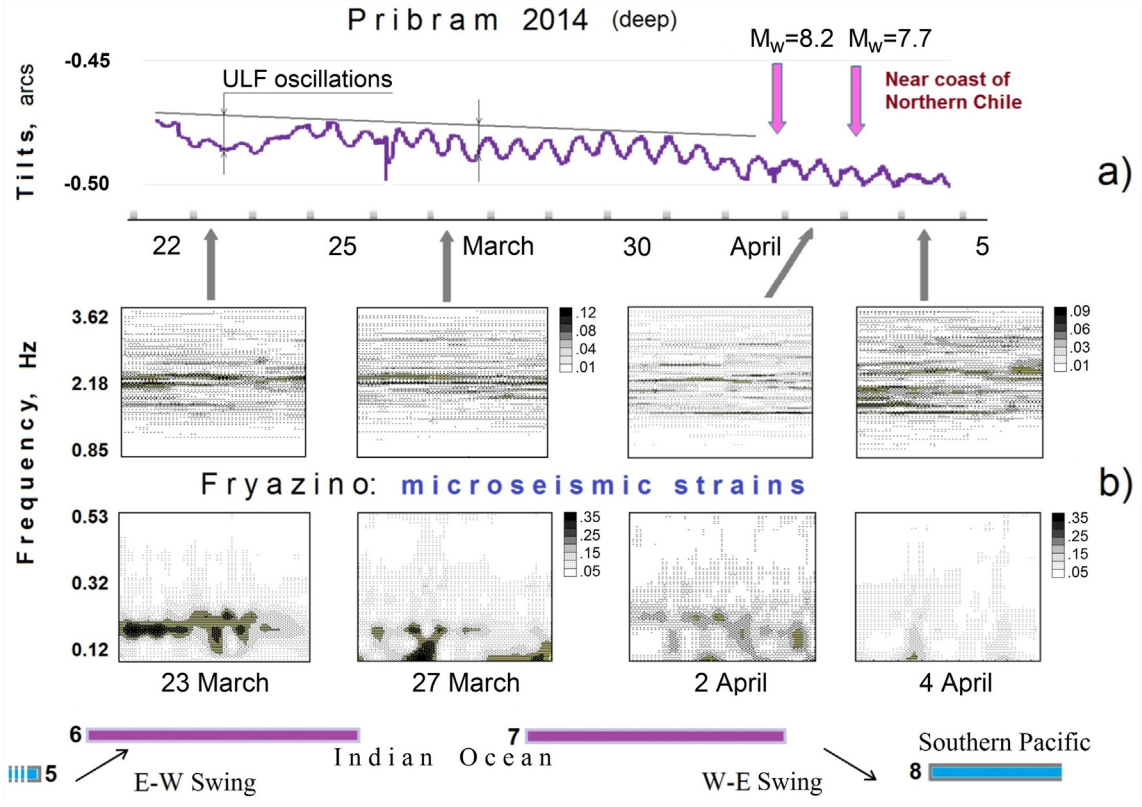

Fig. 9. The tidal tilt perturbations in a deep mine of Pribram (a) and time-frequency evolution of seismic strain oscillations in Fryazino site (b) together with tropical cyclone activity in Southern Pacific: LUSI - 5, ITA - 8 and in Indian Ocean: GILLIAN - 6, HELLEN - 7.

Table 4
Tropical cyclones, typhoons and storms in January–April, 2014 [43,50].

Name	Category	Duration	Basin
BEJISA	3	01–05 January	Indian Ocean
IAN	4	05–13 January	Southern Pacific
COLIN	4	09–15 January	Indian Ocean
LINGLING	–	10–20 January	NW Pacific
DELIWE	–	16–18 January	Indian Ocean
JUNE	–	17–19 January	Southern Pacific
DYLAN	–	29–31 January	Southern Pacific
KAJIKI	–	29 January–01 February	NW Pacific
EDNA	–	04–05 February	Southern Pacific
EDILSON	–	05–07 February	Indian Ocean
FOBANE	–	06–14 February	Indian Ocean
GUITO	1	17–22 February	Indian Ocean
FAXAI	1	27 February–03 March	NW Pacific
KOFI	–	01–03 March	Southern Pacific
LUSI	1	07–14 March	Southern Pacific
GILLIAN	5	06–25 March	Indian Ocean
HELLEN	4	26 March–05 April	Indian Ocean
ITA	4	01–14 April	Southern Pacific
JACK	2	15–22 April	Indian Ocean

[39] ($M_S = 7.9$ according to CEME estimations [38]) on the 1 April 2014 was the strongest one in 2014.

At the end of March 2014, tilt observations in Pribram continued in an old mine at a depth of 90 m (see Section 3). The comparison of observation results from Pribram tiltmeter during 22 March – 04 April with micro-seismic strains in Fryazino together with tropical cyclone performances in Southern Hemisphere is presented in Fig. 9.

Irregular and disturbed trend of about 1.4 mas/day was observed by tiltmeter (Fig. 9a). Peak-to-peak amplitudes of the semidiurnal tidal waves, being less than 2 mas in their minimum on 24 March (Last Quarter Moon), reached maximum value of near 10 mas on 30 March (New Moon). Two and four days later, the two strongest (01 April 2014, M_W8.2 and 03 April 2014, M_W7.7, see Table 3) earthquakes occurred near the coast of Northern Chile, respectively. Pre-seismic tilt disturbances in form of intensive ULF oscillations, mounting up to 1–2 tidal amplitude with frequencies lower than 0.006 mHz, had been observed during 23–27 March in Pribram (see the beginning of diagram in Fig. 9a).

The time-frequency analysis results with high temporal resolution for micro-seismic strains recorded at Fryazino site on 23 March, 27 March, 2 April and 4 April 2014 (Fig. 9b) are shown in form of 4 couples of time-frequency diagrams in frequency bands of 0.12–0.53 Hz and 0.85–3.62 Hz.

"Burst" and moderate synchronizations of 0.15–0.2 Hz micro-seisms (two lower diagrams in the left of Fig. 9b) were observed during 23–27 March 2014. This performance corresponds to the intensive pre-seismic tilt ULF oscillations in Pribram (see Fig. 9a). This process was followed by high coherent synchronization of 1–3 Hz micro-seismic strains, namely, sharp contraction of spectral components shown on the upper 2nd and 3rd time-frequency diagrams (Fig. 9b). "Burst" and synchronization processes were finished on 04 April 2014 after the M_W8.2 and M_W7.7 earthquakes.

In comparison with tropical cyclone activity in January–February 2014, the tropical cyclone activity during March–April 2014 had a considerable growth in Indian Ocean and Southern Pacific (see Table 4). Cyclone activity (tropical storm FOBANE and cyclone GUITO) was shifting from boundaries of African and Indo-Australian plates to Pacific plate. Typhoon FAXAI, tropical storm KOFI and cyclone LUSI were developed in NW Pacific and Southern Pacific from 27 February to 14 March. The most powerful tropical cyclone GILLIAN (Category 5) during 23–24 March 2014 reached its peak intensity above the West Australian Basin. Intensive tilt ULF oscillations in Pribram and "burst" of 0.15–0.2 Hz microseisms in Fryazino were observed in those days.

Activity regions of the next two intensive cyclones HELLEN and ITA (both, Category 4) continued the W–E swings in wide spatial range: the powerful atmosphere–ocean disturbances from SW Indian Ocean (Mozambique Channel) to SW Pacific (Solomon Sea). This process called force an exciting of the African, Indo-Australian and Pacific tectonic plates, which looks like the rolling and pitching of a boat. The preceding Southern Pacific cyclones (KOFI and LUSI) transmitted a "baton" to Indian Ocean cyclones (GILLIAN and HELLEN), which in turn give way to SW Pacific cyclone ITA (the later four of these cyclones shown by the badges 5–8 at the bottom in Fig. 9).

It is necessary to mark the particular track of tropical cyclone HELLEN accompanied by the Chile M_W8.2 earthquake. Southeastward motion of this cyclone (from African continent to Madagascar) rapidly changed to the southwestward at 06:00 UTC on April 1 when it was contiguous to the island [44]. Being about 12,000 km apart from the epicenter, the distinguished atmosphere–ocean interaction with the Earth's surface happened 18 h before the M_W8.2 earthquake.

The occurrence times of Chile M_W8.2 and M_W7.7 earthquakes were just fallen into the period between Indian Ocean cyclone dissipation and SW Pacific cyclone arising, which was mentioned in the previous cases (Fig. 8 and Section 4). So, we assume SW Indian Ocean cyclone GUITO (17–22 February) and NW Pacific typhoon FAXAI (27 February – 03 March) to be the driving source of the Chile M_W8.2 (1 April 2014) and Solomon Islands M_W7.6 (12 April 2014, Table 3) earthquakes.

Unfortunately, we had not obtained continuous tilt records in April due to unstable instrument operation. Nevertheless, we should note that ITA (Southern Pacific) and JACK (Indian Ocean) were the last intensive cyclones, which closed the 2013–2014 Southern Pacific and Indian Ocean cyclone seasons and accompanied the series of four interplate $M_W > 7$ Solomon Islands earthquakes (see Tables 3 and 4). It is worth noting that intricate trajectory of cyclone ITA motions has its origin in Solomon Sea [44], being less than 200 km away from the epicenter of the 12 April M_W7.6 earthquake. This event is the strongest one among the mentioned 9-day series of earthquakes within the close region near Pacific – Australian plate boundary (Table 3, Fig. 5).

As a result, both examples of cyclone–earthquake interaction (Figs. 8 and 9) are consistent with the performances of all previously analyzed events (Section 4). The phenomenon obeys the following rule. The process of interaction began 1–2 months before an earthquake. The W–E and E–W, or S–N, SW–NE and other spatial and temporal swings of tropical cyclone occurred in form of spatial changing the regions of tropical cyclones origins as well as the ocean basins of their activity. The further strengthening of cyclones accompanied a wide range of precursory phenomena that can be recorded at a distance of up to 10^3–10^4 km. The term of cyclone dissipation and its activity transferring to another oceanic basin implies the expected occurrence time of strong earthquake with a maximum probability. In particular, an earthquake does not occur at a moment of peak intensity of hurricane or typhoon but only in its arising or decreasing stage. The observed temporal retardation and outstripping could be accounted for by integral and differential relationships between time-dependent physical processes, which describe the observed phenomena.

The mathematical analysis of the recorded processes will detect a physical pattern of tropical cyclone and earthquake interaction. In order to determine the probable influence of tropical cyclones (hurricanes, typhoons) on occurrence time of earthquake, three main mechanisms should be considered.

Firstly, the quasi-static surface loadings initiate the normal up and down deformations due to significant atmospheric depressions ($\Delta p \geq 100$–200 mbar) in the active zones of strong hurricane or

super typhoon. The strain-baric coefficient was $2\cdot10^{-8}$–$2\cdot10^{-9}$ mbar^{-1} at the depth of 2–15 m under earth surface [21]. With the increase of depth, the strain-baric coefficient was reported to be $5\cdot10^{-10}$ mbar^{-1} in a 1 km deep tunnel [22]. Therefore, strong cyclone can generate a volumetric strain $\Delta V/V$ of an order of ~10^{-8}, which is about the level of tidal strain or the time-dependent tectonic deformation in the tidal frequency band at seismogenic depths. This forthright spheroidal loading on the seafloor is significant enough to trigger an earthquake, namely, the dip–slip event may start up.

The swings of cyclone activity regions between the adjacent plates of the Earth's crust can reinforce the influence of surface loading. The deep atmospheric depression that moves close to the plate boundary can generate the uplifting forces acting on the plate at near border region. This can produce diverse types of bend deformations of the plate tissue giving rise a local stress in lower seismogenic zones of the crust. Meanwhile, stress transfer through the rigid plate body from one side to the other may occur and thus leads to plate subsidence at the border of the other side. So, occurrence of intraplate earthquake is possible.

Secondly, the impact of tropical cyclone consists in its high angular momentum owing to rapid vortex rotation of cyclone system. Conservation of angular momentum of the atmosphere–ocean–lithosphere system may cause considerable growth of interactive torque, which transfers from the tropical cyclone to the earth surface, acts on a coastline and is released through atmosphere–land friction. This happened on April 1, 2014 when the cyclone HELLEN stroke Madagascar. Time-dependent shear strains generated by hurricanes (typhoons) would perform the toroidal loadings that may trigger interplate earthquakes characterized by a strike-slip faulting mechanism.

Finally, storm microseisms, which are the classic manifestation of tropical cyclone, have surely to be taken into account. Hurricanes (typhoons) generate intensive ocean waves, which induce alternate ground motions on the seafloor. Broadband strain oscillations at far distances penetrate into wide depths in lithosphere and arrive in earthquake preparation zone certainly. Oscillating earth strains, which reduce friction and stimulate rock destruction, could be an appropriate factor of triggering earthquake. This justifies frequent appearances of microseisms before strong earthquakes [3,9].

We do not intend to make an exhaustive study and thorough explanation of the above phenomena. Only probabilistic view of the problem was outlined. The detail correlation of temporal characteristics, including their delay and advance as well as more rigorous interrelationships, need further investigations. Endogenic and exogenic factors, including the variations of ionosphere and solar activity, should be taken into account. An integration of precise ground-based instruments with satellite remote sensing systems could be a proper way to solve this problem.

6. Conclusions

The comparison of wideband earth deformations (tilts and strains) data with tropical cyclone activity in the World Ocean in the periods of the strong earthquakes ($M_W = 7$–8) during February and April 2014 approved the correlation of these powerful natural processes. Main features of the newly investigated processes are consistent with the detail analysis of 2004 Sumatra M_W9.1, 2003 Hokkaido M_W8.3 and other strongest earthquakes in 1997–2004.

The daily dissipation energy released by the most powerful tropical cyclone (hurricane, typhoon) is estimated to have same order of magnitude as the energy released by the strongest earthquake ($M_W = 7$–9). This dissipation energy is big enough to trigger an earthquake. The powerful cyclone development, on the other hand, accompanies a wide range of earthquake precursory phenomena that can be recorded at far distances of up to 10^3–10^4 km.

Precise tiltmeter and laser strainmeter, which observe the horizontal components of earth surface deformations, are the proper instruments for study the above mentioned processes. The time-frequency data analysis reveals a behavior of ultra-wideband (0.002 mHz–3 Hz) oscillations associated with tropical cyclone performances. The comparison of the obtained data with anomalous geomagnetic and ionospheric variations comes to an agreement with the observed phenomena. The studied processes look like the excited and powerful disturbances travelling through adjacent geospheres: earth crust – hydrosphere – atmosphere – ionosphere.

The obtained results have allowed the triggering mechanism of an earthquake to be proposed. The process usually begins with the spatial and temporal swings between the regions of origin of tropical cyclones and their activity basins. An intense forcing of lithosphere plates occurs due to significant atmospheric depressions, strong vortex mechanical perturbations and alternating micro-seismic strains. Quasi-static and time-dependent surface loadings produce normal and shear deformations, which initiate the combined spheroidal and toroidal exciting along the coastline and in the seafloor close to the boundary of adjacent tectonic plates. The process of triggering an earthquake may arise. It is an interesting physical phenomenon that an earthquake does not occur at the moment of peak intensity of hurricane (typhoon) but only in its arising or decreasing stage, which is an inherent feature of slow developing processes.

Subsequent investigation and quantitative process modelling should be fulfilled. It is very useful for developing a methodology for early warning of seismic hazard and other natural disasters.

Author statement

The authors of manuscript “Atmosphere, ocean and lithosphere interaction as a possible drive of earthquake triggering” certify that all authors have seen and approved the final version of the manuscript being submitted into the journal “Geodesy and Geodynamics”. They warrant that the article is the authors' original work, hasn't received prior publication and isn't under consideration for publication elsewhere.

Conflicts of interest

The authors declare that there is no conflicts of interest.

Acknowledgments

Some work on recording and processing data in Czech observatory was supported by the CzechGeo/EPOS projects (No.LM-2010008 and LM-2015079).

References

[1] T. Rikitake, Earthquake Prediction, Elsevier Scientific Pub. Co., Amsterdam, New York, 1976, p. 357.
[2] I.L. Nersesov, L.A. Latynina, Strain processes before the Spitak earthquake, Tectonophysics 202 (1992) 221–225.
[3] G.A. Sobolev, Seismicity dynamics and earthquake predictability, Nat. Hazards Earth Syst. Sci. 11 (2011) 445–458.

[4] M. Hayakawa, O.A. Molchanov, T. Ondoh, E. Kawai, The precursory signature effect of the Kobe earthquake on VLF subionospheric signals, J. Commun. Res. Lab. 43 (1996) 169–180.
[5] I. Barnet, J. Procházka, L. Skalský, Do the Earth tides have an influence on short-term variations in radon concentration? Radiat. Protect. Dosim. 69 (1997) 51–60 (Nuclear Technology Publishing).
[6] B.I. Volkov, I.P. Dobrovol'sky, S.I. Zubkov, S.Y. Sekerzh-Zenkovich, Time forms of earthquake precursors, Izvestiya, Phys. Solid Earth 35 (1999) 330–333.
[7] J. Mrlina, A. Špičák, L. Skalský, Non-seismological indications of recent tectonic activity in the West Bohemia earthquake swarm region, J. Geodyn. 35 (2003) 221–234.
[8] V.G. Bondur, V.M. Smirnov, Method for monitoring seismically hazardous territories by ionospheric variations recorded by satellite navigation systems, Dokl. Earth Sci. 403 (2005) 736–740 (Pleiades Publishing, Inc).
[9] M.N. Dubrov, V.A. Alyoshin, A.P. Yakovlev, Wideband laser strainmeters as a new instrument for geophysical research, Gerl. Beitrage Geophys. 98 (1989) 292–300. Leipzig (ISSN: 0016-8696).
[10] H. Benioff, J.C. Harrison, L. LaCoste, W.H. Munk, L.B. Slichter, Searching for the Earth's free oscillations, J. Geophys. Res. 64 (1959) 1334–1337.
[11] G.I. Dolgikh, U.H. Kopvillem, A.N. Pavlov, Observation of periods of free oscillations of the Earth by laser strainmeter, Izvestia Akad. Sci. USSR, Physics of the Solid Earth 19 (2) (1983) 15–20.
[12] L. Petrova, V. Volkov, Dynamic features of seismo-gravitational oscillations of the Earth, in: Transactions (Doklady) of the Russian Academy of Sciences/Earth Science Section 351A, Pleiades Publishing, Inc, 1996, pp. 1477–1480.
[13] N. Kobayashi, K. Nishida, Continuous excitation of planetary free oscillations by atmospheric disturbances, Nature 395 (1998) 357–360.
[14] N. Suda, K. Nawa, Y. Fukao, Earth's background free oscillations, Science 279 (1998) 2089–2091.
[15] K. Nishida, N. Kobayashi, Y. Fukao, Resonant oscillations between the solid earth and the atmosphere, Science 287 (2000) 2244–2246.
[16] V.A. Volkov, M.N. Dubrov, R.F. Matveev, The lithosphere and atmosphere interaction activity and its possible connection with coseismic process, XXII General Assembly of the International Union of Geodesy and Geophysics IUGG 99, Birmingham, 18-30 July, 1999, Abstracts, week A 171 (1999) A.159.
[17] M.N. Dubrov, S.P. Golovachev, Earthquake and hurricane remote monitoring by ground-based interferometry, ISPRS Archives 38 (8) (2010) 254–255.
[18] S. Golovachev, M. Dubrov, V. Volkov, The interaction between the tropical cyclogenesis and seismic activity as derived from spacecraft and ground-based measuring systems, Act. Probl. Remote Send. Earth Space 8 (1) (2011) 232–238 (in Russian with English abstract).
[19] M.N. Dubrov, V.A. Volkov, S.P. Golovachev, Earthquake and hurricane coupling is ascertained by ground-based laser interferometer and satellite observing techniques, Nat. Hazards Earth Syst. Sci. Discus. 2 (1) (2014) 935–961.
[20] V.A. Volkov, M.N. Dubrov, Geodynamical observations using spatially distributed gravimeters, tiltmeters, and laser strainmeters, in: Bulletin d'Information des Marees Terrestres, vol 148, 2014, pp. 11971–11986.
[21] M.N. Dubrov, L.A. Latynina, R.F. Matveev, A.V. Ponomarev, Observation of ultralong-period earth surface strain oscillations attached to the small variations of atmospheric pressure, Izvestiya Phys. Solid Earth 34 (1998) 983–990. Pleiades Publishing (ISSN 1069-3513).
[22] S. Takemoto, H. Momose, A. Araya, W. Morii, J. Akamatsu, M. Ohashi, A. Takamori, S. Miyoki, T. Uchiyama, D. Tatsumi, T. Higashi, S. Telada, Y. Fukuda, A 100 m laser strainmeter system in the Kamioka Mine, Japan, for precise observations of tidal strains, J. Geodyn. 41 (2006) 23–29.
[23] M.N. Dubrov, O.S. Kazantseva, A.B. Manukin, V.I. Ponyatovskaya, The study of synchronously measured variations in the Earth's surface strain and groundwater level, Izvestiya, Phys. Solid Earth 43 (2007) 404–411 (Springer Science+Business Media LLC).
[24] G. Kopp, J.L. Lean, A new, lower value of total solar irradiance: evidence and climate significance, Geophys. Res. Lett. 38 (2011) L01706.
[25] P. Melchior, The Tides of the Planet Earth, 2-nd edition, Pergamon Press, Oxford, New York, 1983, p. 641.
[26] A.V. Kalinina, V.A. Volkov, A.V. Gorbatikov, J. Arnoso, R. Vieira, M. Benavent, Tilt observations in the normal mode frequency band at Geodynamic Observatory Cueva de los Verdes, Lanzarote, Pure Appl. Geophys. 161 (2004) 1597–1611.
[27] B. Košťák, J. Mrlina, J. Stemberk, B. Chán, Tectonic movements monitored in the Bohemian Massif, J. Geodyn. 52 (2011) 34–44.
[28] M.N. Dubrov, V.M. Smirnov, Interdependent perturbations of the Earth's surface, atmosphere, and ionosphere, Geomagn. Aeron. 53 (1) (2013) 49–59.
[29] M.N. Dubrov, P.V. Medvedev, Accurate Laser Interferometer System for Displacement Measurements with 1 Pm Resolution, CAOL 2008, 4th International Conference on Advanced Optoelectronics and Lasers, September 29–October 4, 2008, Alushta, Crimea, Ukraine, 2008, pp. 165–167.
[30] A.V. Nikolaev, A.V. Lukanenkov, M.N. Dubrov, New possibilities of combined data processing from recording of displacements and strains in the field of seismic waves, Dokl. Earth Sci. 430 (2) (2010) 258–260 (Springer – Pleiades Publishing, Ltd).
[31] F. Rolandone, R. Burgmann, D.C. Agnew, I.A. Johanson, D.C. Templeton, M.A. d'Alessio, S.J. Titus, C. DeMets, B. Tikoff, Aseismic slip and fault-normal strain along the central creeping section of the San Andreas fault, Geophys. Res. Lett. 35 (2008) L14305.
[32] A.J. Barbour, D.C. Agnew, Detection of seismic signals using seismometers and strainmeters, Bull. Seismol. Soc. Am. 102 (2012) 2484–2490.
[33] D.C. Agnew, F.K. Wyatt, Dynamic strains at regional and teleseismic distances, Bull. Seismol. Soc. Am. 104 (2014) 1846–1859.
[34] A. Amoruso, L. Crescentini, The geodetic laser interferometers at Gran Sasso, Italy: recent modifications and correction for local effects, J. Geodyn. 48 (2009) 120–125.
[35] S. Takemoto, A. Araya, J. Akamatsu, W. Morii, H. Momose, M. Ohashi, T. Higashi, Y. Fukuda, S. Miyoki, T. Uchiyama, D. Tatsumi, H. Hanada, I. Naito, S. Telada, N. Ichikawa, K. Onoue, Y. Wada, A 100 m laser strainmeter system installed in a 1 km deep tunnel at Kamioka, Gifu, Japan, J. Geodyn. 38 (2004) 477–488.
[36] D. Dontsov, W. Pöschel, W. Schott, N. Kukowski, T. Jahr, P. Schindler, Tidal Earth Crust Deformation Measurements, 58th Ilmenau Scientific Colloquium, Technische Universitat Ilmenau, 08–12 September 2014, p. 9. URN Paper.
[37] T. Jahr, Non-tidal tilt and strain signals recorded at the geodynamic observatory Moxa, Thuringia/Germany, Geod. Geodyn. 9 (2018) 229–236.
[38] Geophysical Survey of Russian Academy of Sciences, Operative Seismological Catalogue, CEME, Obninsk, 2018. http://www.ceme.gsras.ru/cgi-bin/new/catalog.pl.
[39] NEIC/USGS Web-Catalog, US Geological Survey, 2018. http://earthquake.usgs.gov/earthquakes/map/.
[40] L.I. Morozova, Typhoons and seismicity, Dokl. Earth Sci. 410 (2006) 1132–1135.
[41] M.I. Yaroshevich, Intra-annual dynamics of seismic activity in the cyclonic zone of the northwestern part of the Pacific Ocean, Dokl. Earth Sci. 431 (1) (2010) 409–412 (Springer International Publishing AG).
[42] I.V. Pokrovskaya, E.A. Sharkov, Catalog of Tropical Cyclones and Tropical Disturbances of the World Ocean: Chronology and Evolution, Version 2.1 (1983–2005), Poligraph Servis, Moscow, 2006, p. 728.
[43] U. Weather, Archival Hurricane Data from 1851 to 2017. https://weather.unisys.com/hurricanes.
[44] C. Hennon, International Best Track Archive for Climate Stewardship, NOAA NCEI, North Carolina Univ., IBTrACS data - Map and Plots, 2009–2014. http://www.atms.unca.edu/chennon/ibtracs/index.shtml.
[45] J. Jeřábek, B. Chán, L. Skalský, Tidal strain observations at station Lazec, in: Proceedings from Seminary "Advances in Gravimetry", Smolenice, December 10–14, 1990, GI SAS, Bratislava, 1991, pp. 211–216.
[46] Y. Murakami, O. Shimizu, H. Sato, T. Yamada, Sediment-related disaster caused by typhoon 0310 (Etau) in Hidaka region of Hokkaido, Japan, Int. J. Erosion Cont. Eng 1 (1) (2008) 30–37.
[47] A.J. Meltzner, K. Sieh, M. Abrams, D.C. Agnew, K.W. Hudnut, J.-P. Avouac, D.H. Natawidjaja, Uplift and subsidence associated with the great Acech-Andaman earthquake of 2004, J. Geophys. Res. 111 (2006) B02407.
[48] A. Earnest, C.P. Rajendran, K. Rajendran, R. Anu, G.M. Arun, P.M. Mohan, Near-field observations on the co-seismic deformation associated with the 26 December 2004 Andaman-Sumatra earthquake, Curr. Sci. 89 (2005) 1237–1244.
[49] V.M. Smirnov, Solution of reverse problem of ionosphere radio translucence by means of gradient methods, J. Commun. Technol. Electron. 46 (1) (2001) 41–45.
[50] G. Padgett, Monthly Global Tropical Cyclone Summary December 2004, Australian Severe Weather, 2005. http://www.australiasevereweather.com/cyclones/2005/summ0412.htm.
[51] Space Weather Prediction Center, Geophysical Data IZMIRAN, 2014. Moscow Troitsk, https://forecast.izmiran.ru/.

Dr.Victor Volkov, born in 1934., Current position: Senior Scientist of Schmidt Institute of Physics of the Earth of the Russian Academy of Sciences, Address: Bolshaya Gruzinskaya 10, Moscow, 123995, Russian Federation, E-mail address: vav_volkov@mail.ru.